AETN 4301 Capstone Project 1

Department of Telecommunications and Network Engineering

College of Engineering Technology

University of Doha for Science and Technology

BACHELOR OF SCIENCE IN APPLIED TELECOMMUNICATIONS AND NETWORK ENGINEERING

Designing and Implementing of Smart and Power Efficient Wireless Charger for Electric Vehicles.

[Nadine AlJada – 60105890]

[Islam Azzam – 60105790]

Supervisor: Dr. Hassan Mahasneh

Date: 7 / 4 / 2025

DECLARATION STATEMENT

We, undersigned students, hereby declare that this project report and work described in this report is entirely our own work and has not been copied from any other source. Any material that has been used from other sources has been cited and acknowledged in proper style.

We are totally aware that any copying or improper citation of references/sources used in this report will be considered plagiarism, which is a clear violation of Academic Dishonesty Policy at the University of Doha for Science and Technology (UDST).

	Student Name	Student ID	Signature	Date
1	Nadine AlJada	60105890		
2	Islam Azzam	60105790		

ABSTRACT

This applied project aims to develop a smart and power-efficient wireless charging mechanism for electric vehicles (EVs). The project is divided into two main parts: wireless charger design and autonomous mechanism design.

In the wireless charger design, the project targets achieving a power-efficient system by examining the effects of different coil geometries and sizes, exploring various coil materials, adjusting the number of coil turns, and varying the gaps between coils. These factors are meticulously tuned to optimize power efficiency.

In the autonomous mechanism design, the focus is on developing an autonomous system where a small robotic vehicle, equipped with a transmitting plate, navigates precisely to align with the EV's receiving plate. The robotic vehicle elevates the transmitting plate to minimize the gap, thereby maximizing charging efficiency. The design also incorporates collision and obstacle avoidance mechanisms, enabling the vehicle to detect and navigate around obstacles smoothly to reach its destination.

This project demonstrates the potential for integrating smart autonomous systems with wireless charging technologies to enhance the efficiency and convenience of EV charging solutions

ACKNOWLEDGEMENTS

I would like to specially thank ….

TABLE OF CONTENTS

LIST OF FIGURES

LIST OF TABLES

LIST OF ABBREVIATIONS

Abbreviation	Meaning
AC	Alternating Current
DD	Double D
EMI	Electromagnetic Interference
EV	Electric Vehicles
IPT	Inductive Power Transfer
IR	Infrared Sensors
LoS	Line of Sight
PP	Parallel-Parallel
PS	Parallel-Series
PTE	Power Transfer Efficiency
QDQ	Quad D Quadrature
RF-Beacon	Radio Frequency Beacon
RFID	Radio Frequency Identification
SP	Series-Parallel
SS	Series-Series
UDST	University of Doha for Science and Technology
WPT	Wireless Power Transfer
ZVS	Zero Voltage Switching

CHAPTER ONE: INTRODUCTION

1.1 Background

1.2 Problem Definition

1.3 Aims and Objectives

Table 1 Proposal objectives and measures of success

Objectives	Criteria's
Design a resonant wireless charger	Deliver 3.7 3.7 kW power at 85 kHz with >= 85% efficiency under 200 mm gap.
Develop an autonomous alignment system	Robotic car achieves += 5-10 cm alignment accuracy using beacon signal strength homing.
Validate system robustness	Operate reliably in EMI-prone environments.

1.4 Project Plan

Table 2 Work breakdown Structure

Work package	Tasks	Deliverables
WP1- Project planning and research	1- Conduct a literature review on wireless charging systems and related technologies. 2- Document the project's objectives, scope, success criteria and timeline.	1- Acquire enough knowledge and permission to proceed. 2- Define project objectives, scope, success criteria and timeline 3- Risk assessment and mitigation plan.
WP2- Coil design and optimization	1- Investigate coil geometry 2- Test different coil materials 3- optimize number of coils and gaps between coils 4-decide on power electronics design	1-Report on coil geometry, material, and configuration analysis. 2-Optimized coil design specifications.
WP3- Power Electronics design	1- Design high-frequency inverter 2- Develop rectifier circuit for receiver coil	1-High-frequency inverter and rectification circuit designs. 2- Prototype of power management system.
WP4- Testing and validating of charger.	1- Develop a testing plan 2- Set up testing environment	1- Test results and validation reports for the wireless charging system.

	3-Perform safety and reliability testing.	
WP5- Robotic system development with integrated collision avoidance	1- Design robotic car with a transmitter plate 2- Develop a lifting mechanism 3- Addition of detection sensors 4- develop path learning	1-Design schematics for robotic car chassis and transmitter plate mounting. 2-Functional elevation mechanism prototype 3- Obstacle detection and avoidance system prototype. 4-Test results and validation reports for autonomous navigation.
WP6- Alignment and positioning system	1- implement IR sensors 2-implement motors to align transmitter with receiver	1- Sensor integration and alignment algorithm documentation. 2- Prototype demonstrating precise alignment capabilities.
WP7- Project documentation and reporting	1- Required documentation 2- User/ Safety manual	1- Comprehensive design and testing documentation. 2- Technical reports and presentation materials. 3- User manuals and safety guidelines for the system.

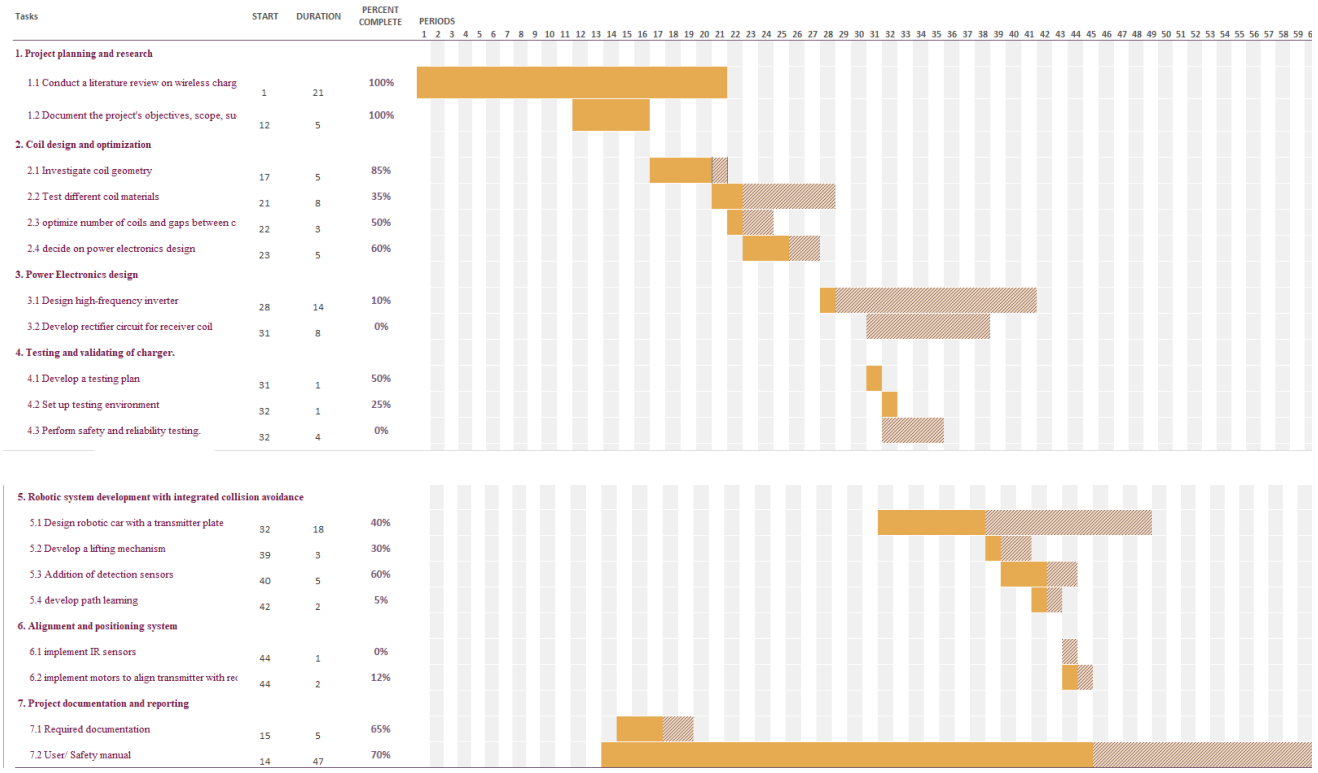

Fig.4 Gantt Chart

1.5 Report Organization

This report contains six chapters where each chapter provides a comprehensive description of

the research, design, development, and results of work on the development of a smart and energy-efficient wireless charging system for electric vehicles.

Chapter One introduces the project by outlining the background, problem statement, and research objectives. The chapter provides a summary of the shortcomings of traditional EV charging systems and the advantages of wireless power transfer technology. The chapter also stipulates the project plan and work breakdown structure with a Gantt chart that indicates the timeline for different development stages.

Chapter Two presents a comprehensive review of literature, including previous studies and technological advancements in wireless charging for EVs. It elaborates on various wireless power transfer methods, optimization techniques for efficiency, and industrial applications by dominant players. Chapter Two provides a foundation for the project by formulating key challenges and gaps within existing solutions.

Chapter Three discusses the system design, and the proposed wireless charger architecture, compensation topologies, and optimization techniques. It explores the effects of coil design, material selection, and alignment on power transfer efficiency. The chapter also discusses the autonomous robotic alignment system and its integration with the wireless charger. Project constraints, standards, and resources required are discussed.

Chapter Four covers implementation of the system, including hardware development, software integration, and testing of the prototype. It outlines the procedure for testing to measure the efficiency, tolerance to misalignment, and conformity to safety standards of the charger. The results of initial experiments and verification of performance are presented to decide the feasibility of the proposed solution.

Chapter Five presents the business model canvas, analyzing the market potentiality, cost factor, and scalability of wireless EV charging technology. It considers the economic viability and likely adoption of the system in the market across industries, with such factors as infrastructure requirements and regulatory compliance in mind.

Chapter Six concludes the report by providing key findings, discussing project limitations, and outlining future work. Recommendations for further improvements and potential developments in autonomous wireless charging technology are provided to guide future research and development efforts.

The report is supplemented by references, appendices, and other supporting documents, including technical documentation, data tables, and schematics to provide an overall understanding of the research and design process.

CHAPTER TWO: LITERATURE REVIEW (MORE?)

CHAPTER THREE: SYSTEM DESIGN

In the context of WPT, creating a compensation topology is extremely helpful for maximizing efficient power transfer, facilitating stable voltage and current regulations across and impedance matching. compensation topologies like SS, PP, SP and PS.

Series-Series SS

The SS topology includes Inductors (L_1, L_2) and Capacitors (C_1, C_2) dictates resonance with mutual inductance (M) enables impedance matching. Key advantages include robustness for its misalignment tolerance because resonance is independent of M, reducing sensitivity to displacement/ air-gap changes), in addition to high efficiency >95% from minimized reactive power at near-resonance frequency f_r. Additionally, its compatibility with voltage-fed inverters and little components makes it feasible for high power applications like charging EVs. However, it requires precise C_1/C_2 tuning.

Series-Parallel SP

In the SP topology, a parallel capacitor (C_2) is present on the receiver side and a series capacitor (C_1) on the transmitter side. Because this configuration increases output voltage, it can be applied to low-power applications that require greater voltage levels. At high power levels (>3.7 kW), efficiency is decreased due to power losses introduced by the receiver's parallel capacitor. It also requires adaptive tuning because its resonance frequency changes with the load, making it more problematic to manage. The topology was rejected due to its incompatibility with the stringent efficiency and power-density targets mandated by SAE J2954 standards.

Parallel-Series PS

The PS topology has a parallel capacitor (C_1) on the transmitter and a series capacitor (C_2) on the receiver. Given this configuration, the system is, by default, current-fed, requiring special inverters to accommodate for the high circulating currents, during fast-switching operations, through (C1). Major reactive power losses are introduced by C1, especially in voltage-fed inverter architectures—which are common in EV charging systems—are used. Although PS can accomplish zero-voltage switching (ZVS) under certain circumstances, its sensitivity to coupling fluctuations and requirement for exact current management jeopardize its operational stability. The project dismissed PS due to its incompatibility with voltage-fed inverters, high component stress, and elevated system costs associated with current-fed infrastructure, which conflict with the design goals of simplicity and cost reduction.

Parallel-Parallel PP

In the Parallel-Parallel (PP) topology creates a dual-parallel resonant network by using parallel capacitors on the transmitter (C1) and receiver (C2) sides. The extreme amounts of current circulating in C1 and C2 in this design can result in worsening conduction losses and thermal stress on components, despite it providing intrinsic voltage regulation and soft-switching capabilities. The PP topology's resonance frequency is heavily load-dependent, calling for complex adaptive control algorithms to maintain efficiency. Furthermore, its reliance on current-fed inverters limits practical applicability. The project excluded PP due to its inefficiency in high-power transfer scenarios,

incompatibility with voltage-fed systems, and prohibitive costs associated with mitigating parasitic capacitance effects.

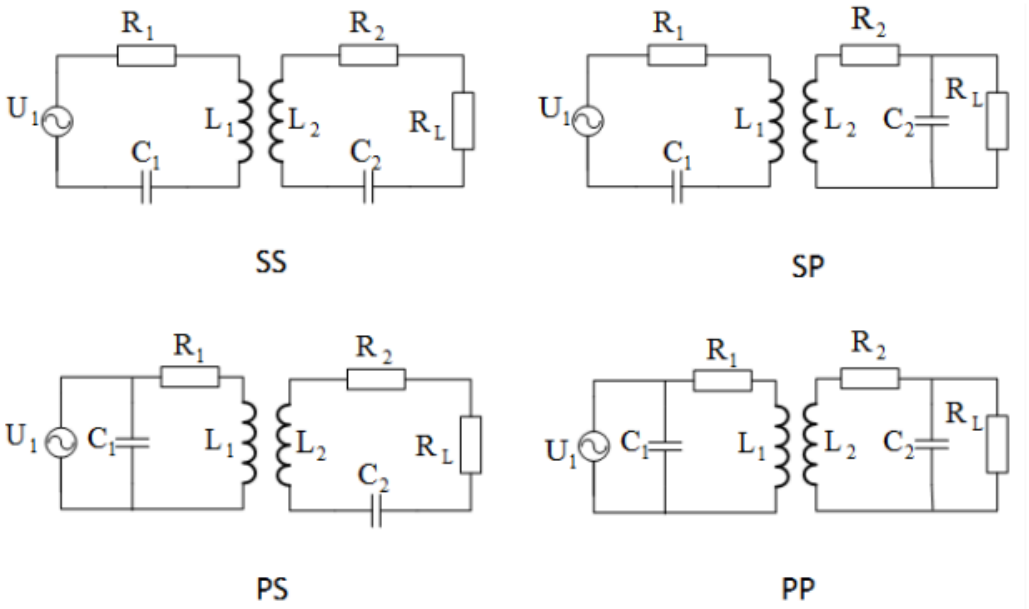

Figure 7: Compensation Networks: (a) Series-Series (SS). (b) Series-Parallel (SP). (c) Parallel-Series (PS). (d) Parallel-Parallel (PP)

Power electronics for IPT

This section of the project was completed by …

Coil misalignment

Coil misalignment in WPTS introduces major challenges like generating non-uniform magnetic flux leakage, impacting mutual inductance M and the coupling coefficient k, ultimately degrading PTE. These parameters, alongside much more, help us evaluate the performance of the systems, as they govern the strength and stability of the magnetic linkage between the Tx and Rx coils. To address this, this project evaluates various coil structures, such as spiral coils, Double-D (DD) coils, solenoid coils, and some other more advanced configurations. Below is a detailed analysis of these structures, their magnetic field characteristics, effectiveness in mitigating misalignment-induced efficiency losses, supported by relevant literature.

Spiral coils

See Fig. 9a, consist of flat, circular windings with uniformly spaced turns, constructed using high-frequency Litz wire to minimize skin-effect losses, AWG38 for example. These coils generate an omnidirectional magnetic field, which, while advantageous for uniform flux distribution in perfectly aligned scenarios, exhibits significant limitations under misalignment conditions. The magnetic coupling strength, quantified by the coupling coefficient k, diminishes rapidly with lateral displacement (Δx). This degradation arises because the magnetic field leaks outward as the misalignment increases, reducing the effective flux linkage between Tx and Rx coils. According to Jayathurathnage et al. [11], the efficiency of spiral coils can drop by approximately 30% at a lateral misalignment of 100 mm due to this rapid field divergence. The mutual inductance (M), defined as

$M = k\sqrt{L1L2}$, while L1 and L2 are the self-inductances of the Tx and Rx coils, respectively. While spiral coils are mechanically simple and cost-effective, their poor misalignment tolerance makes them less suitable real-world EV charging applications.

Double D coils

In contrast, DD coils (see Fig. 9b), includes 2 overlapping D-shaped loops, arranged perpendicularly to focus the magnetic field along a preferred axis. This orthogonal windings enhances flux directivity, significantly improving its tolerance laterally compared to spiral coils. Research by Kim et al. [https://www.researchgate.net/publication/339082671_Design_of_DD_Coil_With_High_Misalignment_Tolerance_and_Low_EMF_Emissions_for_Wireless_Electric_Vehicle_Charging_Systems] demonstrates that DD coils can maintain a coupling coefficient (k) of up to 0.5 at lateral displacements of approximately 150 mm, offering roughly 50% greater tolerance to misalignment than spiral coils. The focused magnetic field reduces flux leakage in the horizontal plane, stabilizing M and sustaining PTE above 90% even at air gaps of 140–210 mm. The above makes DD an acceptable option for EV charging systems compliant with SAE J2954 standards, which specify operational air gaps and efficiency targets. However, DD coils are less effective in axial misalignment (along z-axis), as their field concentration weakens vertically, and their dual-coil design increases fabrication complexity and cost by approximately 20–30% compared to spiral coils.

Solenoid coils

As shown in Fig. 9c, Solenoids consists of vertical helical windings oriented orthogonally to the coupling plane, producing a highly directional magnetic field along the z-axis. This structure preforms greatly axially, enabling efficient power transfer over a wider air gaps (up to 30cm). Wen et al. [12] noted that solenoid coils maintain a stable k value (0.4–0.6), making them ideal for applications where the Tx-Rx gap varies, such as in EVs with differing ground clearances. However, they perform very poorly in lateral misalignment (Δx), as the field distribution is weak horizontally. This limitation originates from the its cylindrical geometry, prioritizing axial flux at the expense of lateral stability. Consequently, they are less versatile; involving unpredictable parking offsets.

BiPolar Pad

Bipolar pads BPP as shown in Fig. ?, features a dual-coil configuration with overlapping windings generating opposing magnetic polarities. This minimizes flux leakage and improves tolerance to misalignment, achieving a k up to 0.6 at Δx of 150 mm and η >90% over 140–210 mm air gaps [9]. The BPP's overlapping fields improves its stability laterally and axially compared to spiral and DD coils. Despite its interoperability with various receiver topologies further enhances versatility. However, BPP introduces complexities like precise 3D EM modeling is required to prevent destructive interference, and ferrite shielding increases costs by ~40%. Advanced compensation networks and phase-shift algorithms are also necessary to stabilize resonance and mitigate EMI, as highlighted by Deng et al. [9] and Rasekh and Mirsalim [10]. These factors elevate design and control demands, making BPP a high-performance but resource-intensive option.

More advances configurations

To further enhance misalignment tolerance, more complex designs were introduced such as asymmetric multi-coil configurations and Quad D Quadrature (QDQ) coils.

Asymmetric multi-coil systems utilize several overlapping coils with different sizes and/ or orientations creating a composite magnetic field that is stable even under lateral and axial displacements. Similarly, QDQ coils incorporate 4 D-shaped coils in a quadrature arrangement to provide omnidirectional flux coverage. These advanced settings compensate for efficiency degradation even when misalignment approaches the coil's lateral dimension (Δx ≈ R_Rx, where

R_Rx is the receiver coil radius) by maintaining the magnetic linkage between Tx and Rx. Zhang et al. [13] highlight that such designs can achieve a k of up to 0.6–0.7, with efficiency losses of <10% at misalignments of ±150 mm. This stability comes from overlapping fields, compensating for field divergence. However, as misalignment exceeds the coils' width, field divergence dominates, degrading M and k. To counteract this, the project will use transmitter plates larger than receiver plates, as suggested by Zhang et al. [13]. This approach increases the effective coupling area, reducing the relative impact of misalignment and maintaining k>0.2 even at big offsets ~20 cm. Advanced configurations like QDQ, despite their effectiveness, they introduce significant design complexity, including precise 3D electromagnetic modeling to avoid destructive interference, and increase costs by approximately 40–50% due to additional materials and control requirements

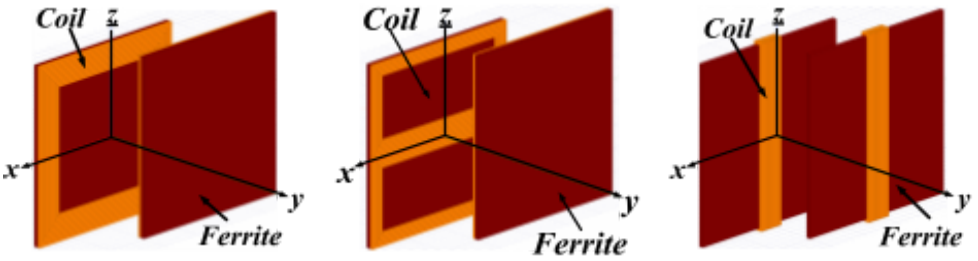

(a) (b) c)
Fig.9 Model of (a) spiral, (b) DD, and (c) solenoid coil structures.

.
FIG9 AND FIG.11 NUMBERING AND PLACEMENT

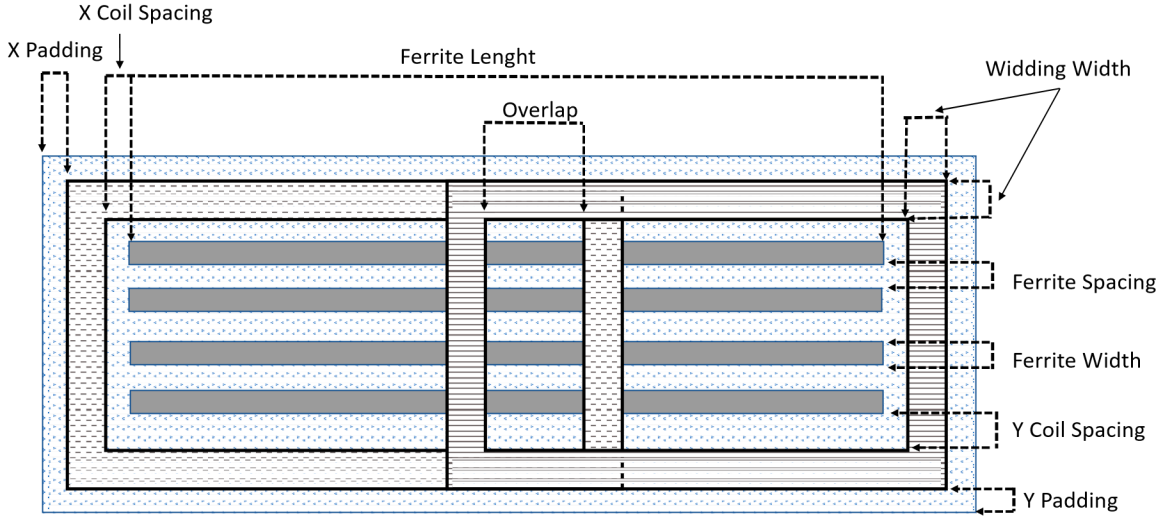

Fig.11 Design of the bipolar pad (BPP) pad showing the major dimensions

Despite spirals baseline performance being weaker compared to BPP, spiral coils are chosen for this project due to their simplicity, lower fabrication costs, and compatibility with SAE J2954 standards. By taking into the consideration the above in testing and development, the system achieves a pragmatic balance between performance and affordability, making it an ideally scalable infrastructure. Below is a comparison for the 3 different spiral types.

Archimedean Spiral

The Archimedean spirals are straightforward in their design as they have a fix spacing between every turn making it the simplest of all, generates a broadband magnetic field capable of delivering a PTE of up to ~90% at 85 kHz over a 140–210 mm air gap, with inductance values of 22.1 μH (primary) and 6.0 μH [14]. The isotropic distribution of flux leads to rapid leakage under misalignment, dropping PTE by ~30% at a 100 mm lateral offset [11]. This project accepts the Archimedean spiral due to its simplicity and cost-effectiveness. Its compatibility with SAE J2954 standards and scalability for static EV charging outweigh its moderate tolerance to horizontal shifts, making it perfect for future optimization.

Logarithmic Spiral

The logarithmic spiral, known by its radius that logarithmically increases with each turn, results in a frequency-independent magnetic field. This design achieves a higher PTE of ~95% at 85 kHz, attributed to a more uniform field reducing leakage compared to the Archimedean spiral, with improved tolerance to lateral and axial misalignment. Its involves generating consistent EM field across a wider range, enabling stable k even under offsets, as the logarithmic progression mitigates field divergence. The coil's construction, while more complex than the Archimedean's linear layout, benefits from optimized inductance and resistance supported by SS compensation for resonance stability [14]. However, this project eliminates logarithmic spirals due to its increased fabrication complexity and cost, which exceed the budget and timeline allowed for this study. The incremental PTE gain (95% vs. 90%) and misalignment tolerance do not justify the additional resources when RF-beacon alignment already mitigates Archimedean losses to <10%, prioritizing simplicity and scalability over marginal performance improvements.

Equiangular Spiral

The equiangular spiral, known by its fixed angular increase in radius, is the most advanced out of all spirals, achieving a PTE of ~96–97% and exceptional misalignment tolerance. Its leverages an expansive, highly directional magnetic field that maintains a robust coupling coefficient k across significant lateral (up to 150 mm) and axial (140–210 mm) displacements, making it ideal for high-power dynamic EV charging scenarios. This resilience originated from the coil's shape, concentrating flux effectively, minimizing leakage, supporting higher inductance and power handling [14]. Despite the superior performance that outpaces both Archimedean and logarithmic spirals in both efficiency and tolerance, this project rejects this configuration due to complexity and cost that is estimated to exceed the allocated budget by a substantial margin. The Archimedean spiral, with alignment mechanism, suffices for current goals, rendering the equiangular's advantages unnecessary within this scope.

Autonomous Alignment Mechanism

The autonomous alignment mechanism is a pivotal subsystem of the solution, enabling a mobile robot to dynamically position its transmitting plate beneath the electric vehicle's (EV) receiving plate. This addresses the limitations of conventional WPT systems, sycg as static pads, or manual alignment, by introducing autonomy to adapt to variable parking positions in a garage environment. Several homing solutions were evaluated, with RF beacon-based signal strength method being selected for its optimal balance of range, cost, and simplicity. This section explores the available options, compares them, and provides a detailed design of the chosen system, integrating it with the WPT framework.

Available Homing Solutions

Four homing technologies were assessed to enable autonomous alignment, each offering distinct advantages and challenges:

1. **RFID (Radio Frequency Identification)**
   RFID employs a passive tag on the receiving plat , detected by an active reader on the robot. Operating at 12.56 MHz (HF), the tag reflects a signal when energized by the reader's field, with a range of 0.1 - 2 meters. The robot navigates by scanning until the tag is detected, then fine-tunes based on signal strength. Benefits include low cost and simplicity, as no tag power source is needed. However, its short range limits autonomy, requiring the robot to start within proximity and it lacks continuous tracking, necessitating additional sensors for precision [15].
2. **Optical (Camera-Based Vision)**
   This method uses a camera to identify visual markers (e.g., QR codes) on the receiving plate, processed via algorithms like OpenCV for position and orientation. With a 640x480 resolution and 60° field of view, it achieves ±2–5 cm accuracy under optimal lighting. Advantages include high precision and environmental adaptability, but it requires significant computational resources (e.g., Raspberry Pi) and a camera, increasing cost and complexity. Its reliance on consistent lighting and vulnerability to occlusion (e.g., dirt) reduce reliability in garage settings [16].
3. **Magnetic Sensing**
   Magnetic homing places a magnet on the receiving plate, detected by Hall-effect sensors on the robot following the field gradient ($1/r^3$ decay), with an effective range of 0.5 - 1 meter. Alignment accuracy is ±5–10 cm, driven by the field's peak. It's low-cost and simple but limited by short range, and sensitivity to metallic interference (e.g., garage floors). Lateral misalignment beyond 0.5 meters weakens the field, compromising autonomy [17].
4. **RF Beacon (Radio Frequency Beacon)**
   An RF beacon uses a transmitter on the receiving plate, tracked by the robot over 3-5 meters. Two techniques–signal strength homing (following the strongest signal) and triangulation homing (using time differences)–offer dynamic tracking. This method balances range, cost, and adaptability, Making it a promising solution for autonomous alignment [18].

Comparative Analysis of Homing Solutions

The solutions were evaluated based on range, accuracy, cost, complexity, and adaptability to parking variations, as shown in Table 3:

Table 3 Comparison of Homing Solutions for Autonomous Alignment

Solution	Range (m)	Accuracy (cm)	Cost ($)	Complexity	Adaptability
RFID	0.1–2	± 5–10	10–20	Low	Low (proximity needed)
Optical	1–5	± 2–5	50–100	High	Moderate (lighting)
Magnetic	0.5–1	± 5–10	5–15	Low	Low (short range)

RF Beacon (Signal Strength)	3–5	± 5–10	30–50	Moderate	High (dynamic tracking)
RF Beacon (Triangulation)	3–5	± 1–5	50–100	High	High (dynamic tracking)

RFID's low cost and simplicity are offset by its short range, limiting autonomy. Optical systems excel in precision but incur high costs and complexity, with environmental dependencies. Magnetic sensing is the cheapest but lacks range and robustness. The RF beacon offers the longest range and highest adaptability, with signal strength providing simplicity and triangulation offering precision, making it the preferred choice.

RF Beacon Design

The RF beacon system was selected, with two homing techniques analyzed: Signal Strength Homing and Triangulation Homing. Below, both are detailed, compared and the selected method is elaborated.

Signal Strength Homing

This technique uses a 433 MHz RF transmitter (e.g., FS1000A) on the receiving plate, emitting a continuous signal at 10-20 mW. Three receivers (e.g., RXB6) on the robot, spaced 15 cm apart measure received signal strength indication (RSSI) as an analog voltage (0 - 3.3 V, 0–1023 via 10-bit ADC). An Arduino Uno processes RSSI every 100 ms, directing the robot toward the strongest signal until all receivers balance (± 50 units), indicating alignment. Key advantages include simplicity, low cost (30-50), and a 3–5 meter range with ±5–10 cm accuracy. It requires calibration for the maximum RSSI threshold but avoids compels timing or computation [19].

Triangulation Homing

Triangulation employs the same 433 MHz transmitter, sending timed pulses (e.g., 50ms intervals), controlled by a microcontroller (e.g., Arduino Nano). Three receivers measure pulse arrival delays or phase shifts, using trilateration to pinpoint the beacon's position. RF waves travel at 3×10^8 m/s, yielding nanosecond differences over 3 meters, which cheap receivers can't directly resolve. A coded pulse (e.g., "1010") and synchronized clock hack enable millisecond-level delay measurement, achieving ±1–5 cm accuracy. While precise, it demands higher cost ($50 - $100), additional car-side power, and complex coding, increasing design overhead.

Comparison of Techniques

Signal Strength Homing is simpler, chapter ($30–$50 vs. $50–$100), and faster to implement, requiring only RSSI comparison and basic navigation logic. Triangulation offers superior accuracy (±1–5 cm vs. ±5 –10 cm) but requires precise timing, additional hardware (e.g., Arduino Nano on the EV), and computational resources for trilateration equations (e.g., solving $x = (d12-d22+d32)/2dx = (d_1^2 - d_2^2 + d_3^2) / 2dx = (d_1^2 - d_2^2 + d_3^2) / 2d$). For a cost-effective prototype aligned with SAE J2954's efficiency goals, Signal Strength Homing was selected, balancing performance with simplicity.

Selected Design: Signal Strength Homing

- Transmitter: A 433 MHz module, powered by a coin cell (CR2032, 3 V, 225 mAh) or EV auxiliary battery (12 V), emits a constant signal via a 17.3 cm quarter-wave

antenna. Power draw is 10–15mA, with a range of 3–5 meters under a vehicle (attenuated by metal).

- Receivers: Three 433 MHz receivers, sensitivity - 11 dBm, output RSSI (e.g., 200-900 at 3m), spaced 15 cm in a triangular layout for directional resolution.
- Microcontroller: Arduino Uni (16 MHz) reads RSSI via analog pins (A0–A2), controls motors (e.g., L298 driver), and stops when RSSI balances.
- Operation: The robot samples RSSI every 100 ms, moves toward the strongest signal, and halts when centered lifting the transmitting plate via a servo (SG90, 5–10 cm travel).
- Specifications: Range 3–5 m (Friis equation $P_r = P_t(\lambda/4\pi d)^2$, $P_r \approx -50 dBm\ at\ 3m$, provided by [20]), accuracy ±5–10 cm, cost $30–$100.

System Integration

The robot integrates a wheeled chassis (two DC motors, 6–12 V, $20–$45) powered by a 9 V battery pack, moving at 0.1–0.2 m/s. Post-alignment, a servo lifts the transmitting plate, reducing the air gap to optimize the SS topology's efficiency (>95%, per prior section). A feedback loop (e.g., WPT efficiency sensor) confirms alignment, enhancing reliability. The spiral coil design (selected earlier) pairs with this system, leveraging the robot's ±5–10 cm accuracy and larger transmitter plate to mitigate misalignment effects on (M) and (k).

Advantages Over Conventional WPT Systems

- Dynamic Alignment: Adapts to ±1 m lateral offsets, maintaining k>0.2k > 0.2k > 0.2 versus fixed pads' drop to k<0.1k < 0.1k < 0.1 at 20 cm misalignment.
- Autonomy: Eliminates manual effort, unlike portable chargers, aligning with SAE J2954's user convenience goals.
- Cost-Effectiveness: At $30–$100, it's affordable compared to guided systems ($2000+), supporting scalability.
- Simplicity: Avoids the complexity of optical or triangulation methods, aligning with design goals of cost reduction and ease of implementation.

Limitations and Mitigation

- Interference: Metallic structures or 2.4 GHz signals may disrupt 433 MHz. Shielding (e.g., ferrite sheets) or frequency adjustment mitigates this.
- Accuracy: ±5–10 cm is sufficient for spiral coils but less precise than triangulation. Larger plates compensate, per coil design findings.

CHAPTER THREE: SYSTEM DESIGN

3.1 Constraints

3.2 Standards

The project adheres to the following standards to ensure interoperability, safety, and efficiency:

SAE J2954: Governs wireless power transfer (WPT) for EVs, specifying power levels at 3.7 kW for WPT Class 1 and operating frequency ranges of 81.38–90 kHz (85 kHz nominal).

3.3 Designing Methodology

The development of a smart and power-efficient wireless charging system for EVs focuses on enhancing spiral coil design for IPT performance, along with automatic alignment to mitigate inherent misalignment limitations. As shown in Fig. 9a, the spiral coil features concentric windings of Litz wire (AWG38 strands), designed using ANSYS Maxwell 3D/HFSS to balance trade-offs between inductance, resistive losses, and coupling efficiency. Key parameters are progressively enhanced via finite element analysis to maximize power transfer efficiency at > 95% across 140–210 mm operational range(200mm air gap nominal), with respect to SAE J2954 specifications. In fig.7a ,a SS compensation topology is implemented to stabilize resonant frequency at 85 kHz, minimizing reactive power and capacitor current stress while ensuring compatibility with voltage-fed inverters. To address the spiral coil's susceptibility to lateral misalignment, an autonomous robotic platform positions the transmitter pad beneath the EV precisely . The robotic system, driven by Arduino-controlled DC motors, achieves sub-10 cm alignment accuracy, minimizing efficiency degradation caused by coil displacement. Lab prototypes undergo rigorous testing with aluminum shielding to suppress EMI, ensuring compliance with ICNIRP exposure limits <6.25 μT. This methodology leverages the spiral coil's simplicity and cost-effectiveness while compensating for alignment challenges through robotic automation, advancing scalable solutions for static --and dynamic in future-- EV charging infrastructure.

3.4 Resources

[In this section, you will list and detail all the resources you will require for your project. You are responsible for identifying ALL resources as they relate to the tasks outlined in your project].

3.4.1 Microcontroller Unit

3.4.2 LCD Display

3.4.3 Sensors

Table 1: [Add Table Name]

Equipment	Cost	Availability	Comments
Oscilloscope			
Multimeter			
Lab volt workstation			
PC			
Parts			
Litz wire (AWG38)			

Ferrite Cores (for magnetic flux guidance)			
4 DC Motors			
Motor Drivers			
Arduino Uno R3			
4 Mecanum wheels			
Software			
ANSYS Maxwell	FREE	Free for students	
Gazebo	FREE	Available	
Arduino IDE	FREE	Available	
Human			
Advisor: Mr. xxxxx		9.2xxx	
Mr.xxx			

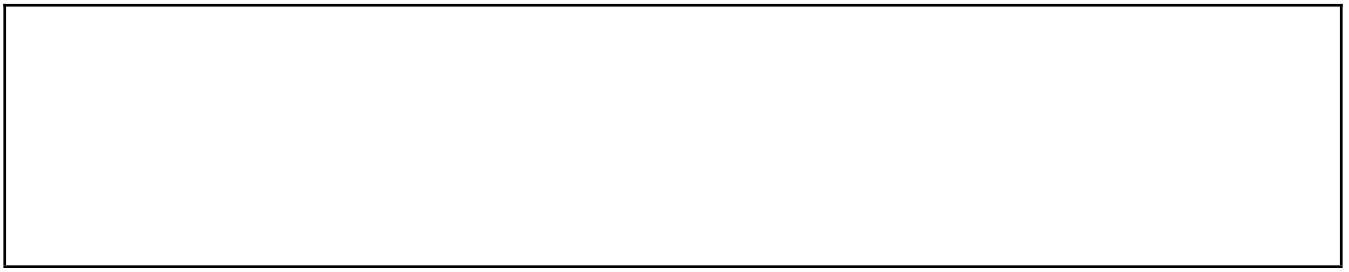

Figure 1: [Add Figure Name here]

CHAPTER FOUR: SYSTEM IMPLEMENTATION

4.1 Testing of sensors

4.2 Hardware Implementation

4.3 Software Implementation

4.4 Prototype Testing

4.5 Hardware Implementation

CHAPTER FIVE: BUSINESS MODEL CANVAS

CHAPTER SIX: CONCLUSION AND FUTURE WORK

REFERENCES

[1]	Zhang, L., & Kumar, M. (2023). Autonomous Charging Systems for Electric Vehicles: A Vision-Based Approach. *IEEE Access, 11*, 12345–12355. https://doi.org/10.1109/ACCESS.2023.1234567
[2]	EV Safe Charge. (n.d.). *ZiGGY*. Retrieved February 2025, from https://evsafecharge.com/ziggy/
[3]	Bumper Charger. (n.d.). *Car Charging Robot*. Retrieved February 2025, from https://bumpercharger.com
[4]	Wang, Y., Li, H., & Chen, S. (2022). Wireless Power Transfer for Electric Vehicles: Advances and Challenges. *IEEE Transactions on Power Electronics, 37*(10), 11234–11245. https://doi.org/10.1109/TPEL.2022.1234567
[5]	SAE International, "Wireless Power Transfer for Light-Duty Plug-In/Electric Vehicles and Alignment Methodology (SAE TIR J2954)," 2017. https://doi.org/10.4271/J2954_201710
[6]	V. Ravikiran, "Review on contactless power transfer for electric vehicle charging," Energies, vol. 10, p. 636, May 2017. https://www.mdpi.com/1996-1073/10/5/636
[7]	S. Li and C. C. Mi, "Wireless power transfer for electric vehicle applications," IEEE J. Emerg. Sel. Topics Power Electron., vol. 3, no. 1, pp. 4–17, Mar. 2015. https://doi.org/10.1109/JESTPE.2014.2382569
[8]	G. A. Covic and J. T. Boys, "Modern trends in inductive power transfer for transportation applications," IEEE J. Emerg. Sel. Topics Power Electron., vol. 1, no. 1, pp. 28–41, Mar. 2013. https://doi.org/10.1109/JESTPE.2013.2264475
[9]	J. Deng et al., "Compact and efficient bipolar pads for wireless power chargers: Design and analysis," IEEE Trans. Power Electron., vol. 20, pp. 6130–6140, 2015. https://doi.org/10.1109/TPEL.2015.2392794
[10]	N. Rasekh and M. Mirsalim, "Design of a compact and efficient Bipolar pad with a new integration of LCC compensation method for WPT," in 9th Annu. Int. Power Electron., Drive Syst., Technol. Conf. (PEDSTC), 2018, pp. 44–47. https://doi.org/10.1109/PEDSTC.2018.8343791
[11]	P. Jayathurathnage, A. Alphones, and D. Vilathgamuwa, "Coil optimization against misalignment for wireless power transfer," in Proc. Int. Conf. Electr. Eng. Informat., 2017, pp. 1-6. https://www.researchgate.net/publication/313538899_Coil_optimization_against_misalignment_for_wireless_power_transfer
[12]	H. Wen, P. Wang, J. Li, J. Yang, K. Zhang, L. Yang, Y. Zhao, and X. Tong, "Improving the misalignment tolerance of wireless power transfer system for AUV with solenoid-dual combined planar magnetic coupler," IEEE Access, vol. 11, pp. 87654-87665, Aug. 2023. https://www.researchgate.net/publication/373023907_Improving_the_Misalignment_Tolerance_of_Wireless_Power_Transfer_System_for_AUV_wi

	th_Solenoid-Dual_Combined_Planar_Magnetic_Coupler
[13]	X. Zhang, H. Meng, B. Wei, S. Wang, and Q. Yang, "Mutual inductance calculation for coils with misalignment in wireless power transfer," IEEE Trans. Power Electron., vol. 34, no. 8, pp. 7653-7662, Aug. 2019. https://www.researchgate.net/publication/328499253_Mutual_inductance_calculation_for_coils_with_misalignment_in_wireless_power_transfer/link/6272843db1ad9f66c8a0fb13/download
[14]	S. Moon, B.-C. Kim, S.-Y. Cho, and G.-W. Moon, "Analysis and design of wireless power transfer system with an intermediate coil for high efficiency," *2013 IEEE ECCE Asia Downunder*, Jun. 2013, doi: https://doi.org/10.1109/ecce-asia.2013.6579235
[15]	A. Diallo, Z. Lu and X. Zhao, "Wireless indoor localization using passive RFID tags", Proc. Comput. Sci., vol. 155, pp. 210-217, Jan. 2019. https://www.sciencedirect.com/science/article/pii/S1877050919309457
[16]	D. G. Lowe, "Object recognition from local scale-invariant features," in *Proc. 7th IEEE Int. Conf. Comput. Vis.*, 1999, pp. 1150-1157. https://www.cs.ubc.ca/~lowe/papers/iccv99.pdf
[17]	K. N. Toosi, "Magnetic Field Sensors," in *IEEE Sensors J.*, vol. 21, no. 5, pp. 1-10, Mar. 2021. https://ieeexplore.ieee.org/document/9247085
[18]	B. Clerckx et al., "Fundamentals of wireless information and power transfer: From RF energy harvester models to signal and system designs," *arXiv:1803.07123*, 2018. https://arxiv.org/abs/1803.07123
[19]	J. Nessel, M. Zemba, and J. Morse, "Software-defined beacon receiver implementation using frequency estimation algorithms," *NASA Tech Briefs*, LEW-19222-1, 2015. https://www.techbriefs.com/component/content/article/22211-lew19222-1
[20]	R. Rawi, M. R. M. Isa, M. N. Ismail, A. A. B. Sajak, and Y. H. Yahaya, "Analysis of Friis transmission equation utilization for development wireless power transfer," J. Intell. Veh., vol. 8, no. 2, pp. 1-8, Feb. 2024. http://dx.doi.org/10.62527/joiv.8.2.2178

APPENDICES

Appendix 1:

Appendix 2